ADVANCED MATERIALS
www.advmat.de

Giant Poisson's Effect for Wrinkle-Free Stretchable Transparent Electrodes

Yan Wang, Qihan Liu, Jianming Zhang, Tianzeng Hong, Wenting Sun, Lu Tang, Eric Arnold, Zhigang Suo, Wei Hong, Zhifeng Ren, and Chuan Fei Guo**

The next generation of flexible electronics will require highly stretchable and transparent electrodes, many of which consist of a relatively stiff metal network (or carbon materials) and an underlying soft substrate. Typically, such a stiff–soft bilayer suffers from wrinkling or folding when subjected to strains, causing high surface roughness and seriously deteriorated optical transparency. In this work, a network with a giant effective Poisson's ratio on a soft substrate is found to be under biaxial tension upon deformation, and thus does not wrinkle or fold, but maintains smooth surfaces and high transparency. Soft tactile sensors employing such network electrodes exhibit high transparency and low fatigue over many stretching cycles. Such a giant Poisson's ratio has the same effect in other systems. This work offers a new understanding of surface instabilities and a general strategy to prevent them not only in flexible electronics, but also in other materials and mechanical structures that require flat surfaces.

Rapid development in the field of flexible electronics has been seen in recent years. Flexible transparent electrodes, which often consist of a conducting but relatively stiff film and a soft substrate, are a key element for flexible photoelectronics, artificial skins, and implantable electronics.[1–7] Typically, a stiff–soft bilayer subjected to compression beyond a critical strain (which is quite small, ≈0.1%) forms instabilities such as periodic wrinkles and deep folds.[8,9] Surfaces with such instabilities are rough, causing dramatically increased haze and low direct optical transmittance of the electrodes,[10–12] as well as poor adhesion,[13–15] which may have adverse effects on subsequent multilayer processing. Therefore, surface instability is a significant problem for flexible transparent electrodes and electronics that require high optical transmittance and a flat surface,[16,17] and it is of great importance to design stretchable electrodes free of surface instabilities. However, flexible electrodes, as well as flexible devices, are required to be employed under various mechanical modes including bending, compression, twisting, stretching, or being subjected to prestrain in order to improve their stretchability, and all of these deformation modes induce anisotropic compressive strains that can easily exceed the critical wrinkling strain and thereby generate surface instabilities. For example, uniaxial stretching generates tension along the elongation direction, whereas in the perpendicular direction the smaller Poisson's ratio of the top conducting layers will lead to a smaller lateral contraction than that of the substrate, thereby causing in-plane compressive stresses and surface instabilities in the top layers.[18] Therefore, the flexible electronics community urgently needs a strategy that can prevent surface instabilities in flexible or stretchable bi/multilayered electrodes and devices, as well as find novel structure designs for wearable and biocompatible flexible devices. [19–21]

In this study, we describe a general design strategy to achieve wrinkle-free stretchable electrodes and devices by introducing a network structure with a large Poisson's effect into

Y. Wang, Prof. J. Zhang, T. Hong, W. Sun, Prof. C. F. Guo
Department of Materials Science and Engineering
Southern University of Science and Technology
Shenzhen, Guangdong 518055, China
E-mail: guocf@sustech.edu.cn

Y. Wang, Prof. J. Zhang, Prof. C. F. Guo
Centers for Mechanical Engineering Research and Education at MIT and SUSTech
Southern University of Science and Technology
Shenzhen, Guangdong 518055, China

Dr. Q. Liu, Prof. Z. Suo
School of Engineering and Applied Sciences
Kavli Institute for Nanobio Science and Technology
Harvard University
Cambridge, MA 02138, USA

Dr. L. Tang, Prof. Z. Ren
Department of Physics and TcSUH
University of Houston
TX 77204, USA
E-mail: zren@uh.edu

E. Arnold
Burdette Keeland Jr. Design Exploration Center
College of Architecture and Design
University of Houston
TX 77204, USA

Prof. W. Hong
Department of Mechanics and Aerospace Engineering
Southern University of Science and Technology
Shenzhen, Guangdong 518055, China

The ORCID identification number(s) for the author(s) of this article can be found under https://doi.org/10.1002/adma.201902955.

DOI: 10.1002/adma.201902955

a network–elastomer bilayer so that surface instabilities may be suppressed during bending, stretching, or releasing from prestretch. The underlying mechanism is the large Poisson's effect of the network that results in a lateral contraction larger than that of the substrate, leading to a biaxial tension state that prevents wrinkling. This strategy is size-independent, and our experimental results show that on the nanoscale, a transparent gold-nanomesh–poly(dimethylsiloxane) (AuNM–PDMS) bilayer electrode is free of wrinkles when released from a large prestrain of up to 100%, while exhibiting significantly improved stretchability and little change in transparency. Likewise, a stretchable capacitive-type tactile sensor employing such electrodes works stably at 100% strain over 1000 cycles. The same mechanism works for a variety of network geometries and the principle can be extended to other electrodes, devices, and systems that are not discussed here. Our method paves a way toward the general predictable design of wrinkle-free flexible electrodes, electronic devices, and other structures or devices in which flat surfaces are preferred.

A metal/elastomer bilayer under compression beyond a critical strain often wrinkles. Since the critical strain is small (≈0.1%)[8,9] compared to the typical working strains of stretchable devices, we simplify the critical condition by assuming that any compressive strain would cause wrinkling. Two typical actions that may easily cause surface instabilities are considered: 1) placing the mesh on a prestretched substrate followed by releasing the substrate, which is a commonly used method to improve the stretchability of electrodes; and 2) biaxially stretching a mesh/elastomer bilayer, which easily generates lateral compression in common situations.

The critical strain for surface instabilities (e.g., wrinkles) ε_c is usually dependent on the elastic properties of the substrate and the film, i.e., wrinkles could be prevented if the applied strain in the film $\varepsilon > \varepsilon_c(E_f/E_s)$, with E_f and E_s being the moduli of the film and substrate, respectively, and negative compressive strain. Wrinkles could be prevented if the lateral strain of the film ε, relative to the substrate, is always tensile, and thus $\varepsilon > 0 > \varepsilon_c(E_f/E_s)$. To achieve this, we propose patterned films with very large Poisson's ratio such that in a freestanding state the lateral shrinkage of the film is always larger than that of the substrate. It is expected to be under lateral tension when bonded to the substrate, and thus free of wrinkles.

Here we used a AuNM–PDMS bilayer, which is a highly stretchable electrode, to study this issue. A typical micromorphology of the AuNM is displayed in **Figure 1**a, which shows a network with an average mesh size of ≈ 1 μm and serpentine nanowires. The PDMS substrate is first stretched along the *x*-direction (Figure 1b, Steps (1) to (2)). The mesh is then transferred to the prestretched PDMS substrate (Step (3)) and the PDMS substrate is subsequently released (Step (4)). Since the mesh is very thin, its deformation is fully determined by the PDMS substrate, and the effect of the mesh on the substrate is minimal. The state of strain is kinematically determinate. If λ_{pre} is the prestretch in the *x*-direction, then the lateral in-plane stretch is $(1/\lambda_{pre})^{1/2}$ in the *y*-direction due to volume incompressibility of the PDMS substrate. Conversely, when the PDMS substrate is released, the stretches of both the AuNM and the substrate are $1/\lambda_{pre}$ in the *x*-direction and $(\lambda_{pre})^{1/2}$ in the *y*-direction with respect to the prestretched state.

To determine whether the AuNM will wrinkle in Step (4), imagine an identical AuNM in a freestanding state and undergoing the same deformation as the substrate in the *y*-direction, with stretch $\lambda_y = (\lambda_{pre})^{1/2}$, but deforming freely in the *x*-direction. For the case that the contraction of the freestanding AuNM mesh (with an original size of $1/\lambda_{pre} \times \lambda_{pre}^{1/2}$) is more than that of the substrate in the *x*-direction, ($\lambda_x < 1/\lambda_{pre}$ or the width $w < 1$) (Figure 1c), the bonded AuNM will be stretched to a size of 1×1 because in reality it fully covers and codeforms with the substrate, and it is under biaxial tension and will not wrinkle. On the other hand, if the contraction of the freestanding AuNM is less than that in the substrate ($\lambda_x > 1/\lambda_{pre}$, or $w > 1$) (Figure 1d), the mesh will be squeezed to match the size of the substrate (1×1), compression is expected in the *x*-direction of the bonded AuNM and wrinkling will occur. This criterion may be expressed in terms of the effective Poisson's ratio, which is defined as the ratio between the nominal strains

$$\nu_f = -\frac{\varepsilon_x}{\varepsilon_y} = \frac{1-\lambda_x}{\lambda_y - 1} \tag{1}$$

To prevent wrinkling, the effective Poisson's ratio of the AuNM needs to satisfy

$$\nu_f > \nu_c = \frac{1-\lambda_{pre}^{-1}}{\sqrt{\lambda_{pre}} - 1} \tag{2}$$

At a small prestrain (λ_{pre} approaching 1), the critical effective Poisson's ratio is 2, and it gradually decreases with increasing λ_{pre} and asymptotically approaches $(\lambda_{pre})^{-1/2}$ when λ_{pre} is large.

Because the effective Poisson's ratio of a freestanding AuNM cannot be easily measured at the nano- or microscale, macroscale kirigami meshes were used to determine the effective Poisson's ratio of the AuNM. It should be noted that in the elastic range, the deformation or the Poisson's effect is highly structure-dependent but insensitive to the mechanical properties of the materials.[22,23] It is therefore expected that the effective Poisson's ratio of a paper mesh is close to that of the AuNM of similar geometry. Here we laser-cut a kirigami structure such that its silhouette (**Figure 2**a) mimics the scanning electron microscopy (SEM) image of an AuNM, and determined the effective Poisson's ratio of the paper mesh by stretching it and recording the ratio between nominal strains in width and length (Figure 2b; Figure S1, Supporting Information) according to Equation (1). To study the effect of the in-plane geometry of the mesh, we changed the mesh size (M) to line width (W) ratio of the paper kirigami. The aspect ratio of mesh ligaments M/W can be determined by analyzing the Fourier transformation pattern of the meshes, which consists of two characteristic reflection rings representing the mesh diameter (M, corresponding to the inner ring) and the line width (W, corresponding to the outer ring) of the ligaments (Figure S2, Supporting Information). The value of M/W is estimated from the reciprocal ratio of the corresponding diameters. The measured effective Poisson's ratios of the paper meshes with M/W aspect ratios of 10, 6, and 4 are found to be significantly larger than the critical value before dense cracks are generated (Figure 2c), indicating that the prestretched AuNM will not wrinkle on a prestretched substrate, and is well beyond the allowable range

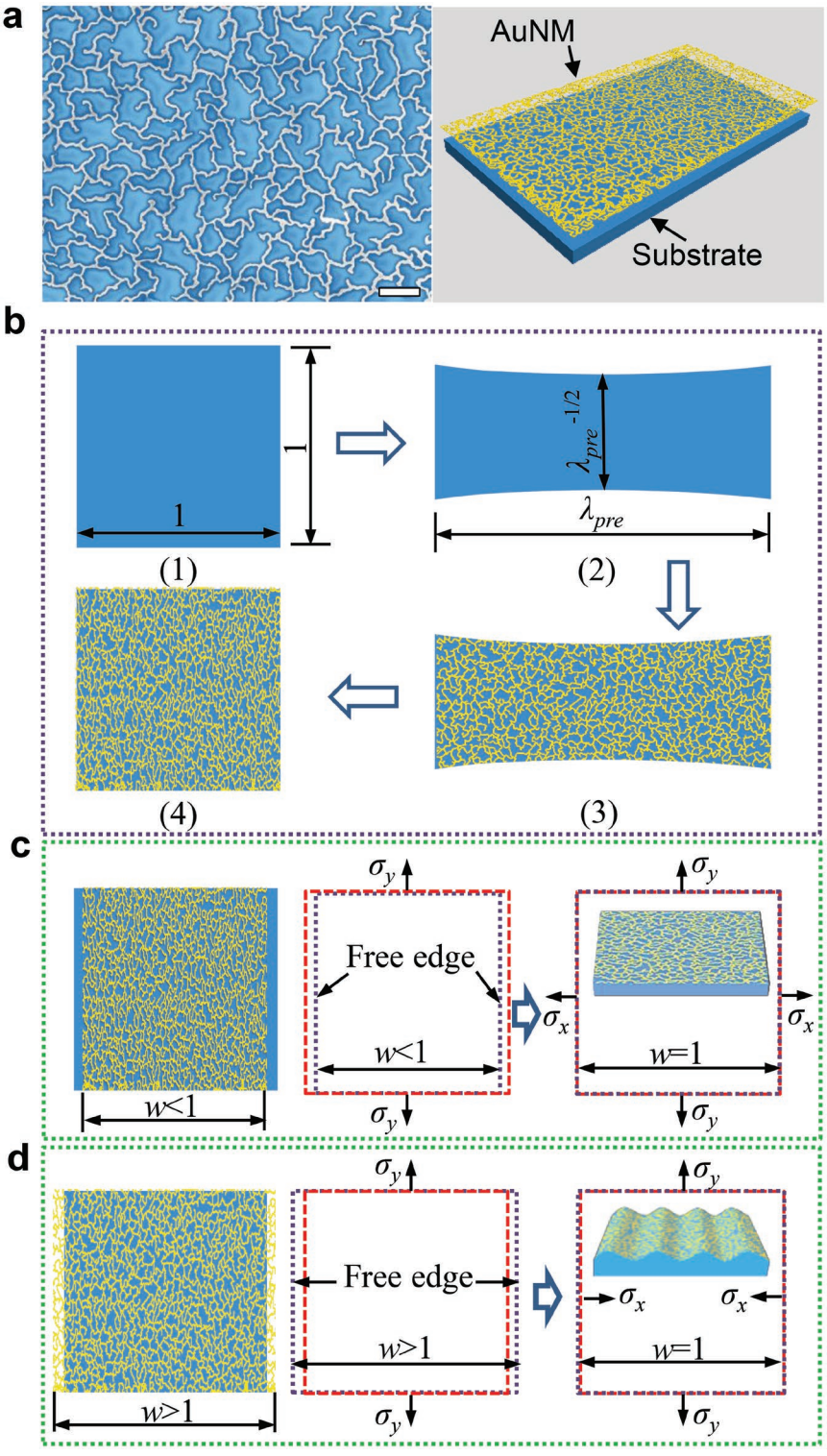

Figure 1. SEM image of AuNM and the mechanism for wrinkle-free electrodes under prestretch. a) A representative scanning electron microscopy image of AuNM. Scale bar: 1 µm. b) Schematic of a mesh on a prestrained elastomeric substrate. The process consists of four steps: Steps (1) and (2): stretching the PDMS substrate with unitless dimensions 1 × 1; Steps (2) and (3): transferring the AuNM; and Steps (3) and (4): releasing. c) The stress state of the mesh when it has a large lateral contraction ($w < 1$). No wrinkles form since the mesh is under biaxial tensile stresses. d) The stress state of the mesh when the mesh has a small lateral contraction ($w > 1$). Wrinkles form because of the compressive stresses along the *x*-direction.

of the Poisson's ratio from –1 to 0.5 in anisotropic solids.[24]

The in-plane stretchability of kirigami structures is known to be accommodated by large out-of-plane deflection. Due to the low bending stiffness, a ligament in the transverse direction of the stretch will be bent out-of-plane when the two ends are sheared in different directions (Figure S3, Supporting Information). The compatibility between neighboring ligaments, on the other hand, induces localized twisting near the two ends of a ligament. Both bending and twisting shrink the ligament span and contribute to the Poisson's effect of the mesh structure. As the size of the twisting regions scales with the width of the ligament (Figure S3, Supporting Information), a wider ligament will need larger twisting regions to accommodate the transition, leaving a shorter middle part for bending, and thus inducing more significant out-of-plane deflection, which shortens the middle part more for the same axial stretch. It is expected that for meshes of the same thickness and similar patterns, those with smaller aspect ratios will manifest larger effective Poisson's ratios. As a result, the effective Poisson's ratio of the freestanding paper mesh is dependent on the aspect ratio *M*/*W*. This geometry dependence is confirmed by our measurements on the freestanding paper meshes: the meshes with *M*/*W* ratios of 4, 6, and 10 have Poisson's ratios of ≈4.5, 3, and ≈2, respectively, in the case of a relatively small prestretch λ_{pre} (≈1.1) (Figure 2c). These meshes all fall within the nonwrinkling regime in the elastic range. As expected, the meshes with larger *M*/*W* ratios (*M*/*W* = 10 and 6) are found to be free of surface wrinkles with a large prestretch λ_{pre} = 2.0, as indicated in our optical microscopy and SEM images (Figure 2d,e).

The above analysis assumes elastic deformation of the ligaments without damage, but in reality, the meshes tend to be torn from the connection regions where stress is concentrated (Figure S3, Supporting Information), especially for those with smaller aspect ratios. Cracks would form even when the mesh is stretched to a relatively smaller strain (λ_{pre} = 1.8), and the

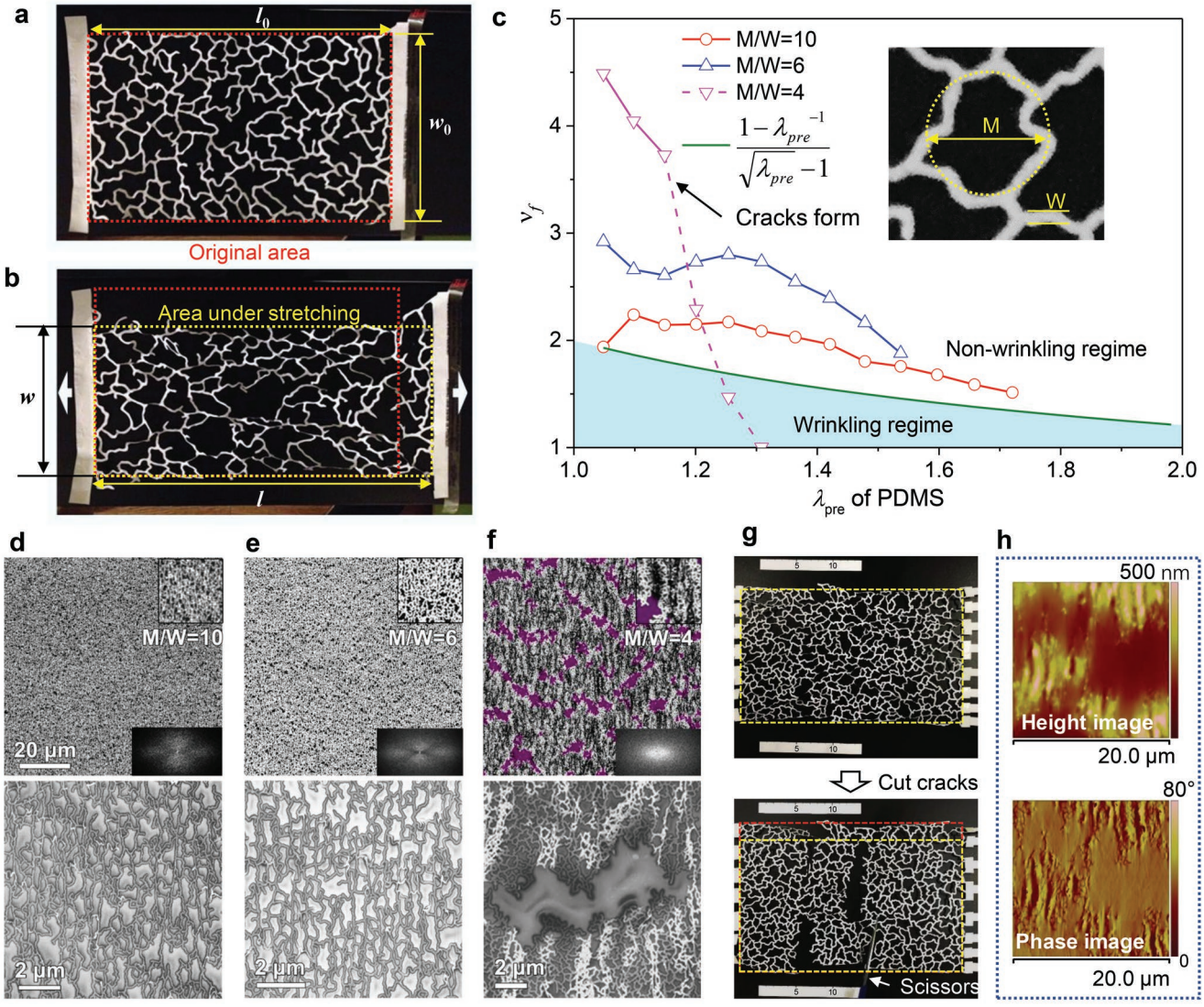

Figure 2. Effective Poisson's ratio of the mesh and the effect of aspect ratio and cracking. a) A paper mesh with dimensions of $l_0 \times w_0$. b) The dimensions of the mesh change to $l \times w$ upon stretching. c) The measured effective Poisson's ratios of meshes with different aspect ratios, all of which are larger than the critical value defined in Equation (2). The inset shows the lengths measured for the *M*/*W* ratio calculation. d–f) Optical (top) and SEM (bottom) images of prestrained ($\lambda_{pre} \approx 2$) AuNMs with *M*/*W* ratios of 10, 6, and 4, respectively. It can be seen that cracks and surface instabilities are formed in the mesh with the smallest *M*/*W* ratio. Lower insets in the optical images show Fourier transformation patterns of the respective meshes, indicating an anisotropic feature of the prestrained AuNMs. Upper insets show magnified images. g) Lateral contraction of a stretched paper mesh decreases as cracks are introduced by using a pair of scissors. h) AFM height and phase images of a AuNM when uniaxially stretched to $\lambda \approx 2.4$, showing cracks and surface wrinkles.

effective Poisson's ratio is sharply reduced (the dashed line with inverted magenta triangles in Figure 2c) due to the relief of axial stretch by the cracks. When a similar AuNM is bonded to a PDMS substrate, wrinkles would be generated upon the formation of the dense cracks (Figure 2f). A similar effect is observed in the paper mesh when cracks are intentionally introduced by cutting some slits with a pair of scissors (Figure 2g).

The working principle is evident: the network itself should possess a giant Poisson's effect together with a large elastic limit (or large stretchability) to be wrinkle-free. It should be noted that due to the flaw insensitivity at the nanoscale, metallic ligaments are expected to withstand a larger strain than macroscopic paper kirigami.[25] As a result, the effective Poisson's ratio of nanoscale metal meshes will be larger than that of corresponding paper kirigami at large strains (beyond the elastic limit of the paper mesh). In addition, this principle is not limited to the mesh structure discussed above, but is also valid for other geometries. For example, a prestretched perforated metal film (which also possesses a large effective Poisson's ratio) made using a phase-separation method would develop dense surface wrinkles perpendicular to the cracks (Figure S4, Supporting Information). Besides prestretching, the effect of cracks is also seen in other mechanical modes, such as uniaxially stretching a bilayer. For example, distributed cracks would form in a AuNM–PDMS bilayer stretched to a large nominal strain ($\lambda = 2.4$), indicating that the real strain in the network is

far smaller than the applied strain, and periodic wrinkles would thereby form as illustrated by the atomic force microscopy (AFM) images in Figure 2h.

For the case when no prestretch is applied to the elastomer substrate, the critical effective Poisson's ratio is 0.5, i.e., that of the incompressible elastomer, that is, the effective Poisson's ratio of the mesh should be larger than that of the substrate to cause a larger lateral contraction in the mesh. The detailed analysis for uniaxial stretching is provided in Figure S5 (Supporting Information) in the Supporting Information. Since the case with prestretch requires a larger critical effective Poisson's ratio, we conclude that a film would be wrinkle-free whenever the effective Poisson's ratio is larger than $\frac{1-\lambda_{pre}^{-1}}{\sqrt{\lambda_{pre}}-1}$. In the small strain range, the effective Poisson's ratio should be no smaller than 2 to avoid wrinkling. The effect of the giant Poisson's ratio is also valid in other mechanical modes such as bending, which often produces much smaller strains than stretching.

Achieving a wrinkle-free film on a prestrained substrate is of great significance. Using a prestrained substrate is a commonly used method to improve the stretchability of electrodes, but it generates wrinkles and results in the seriously adverse effects of rough surfaces and low transmittance.[26–29] Here, the prestrained electrode with a giant Poisson's effect exhibits improved stretchability but little change in transmittance. **Figure 3**a shows that prestretching significantly improves the stretchability of the electrode: AuNMs with larger prestrains

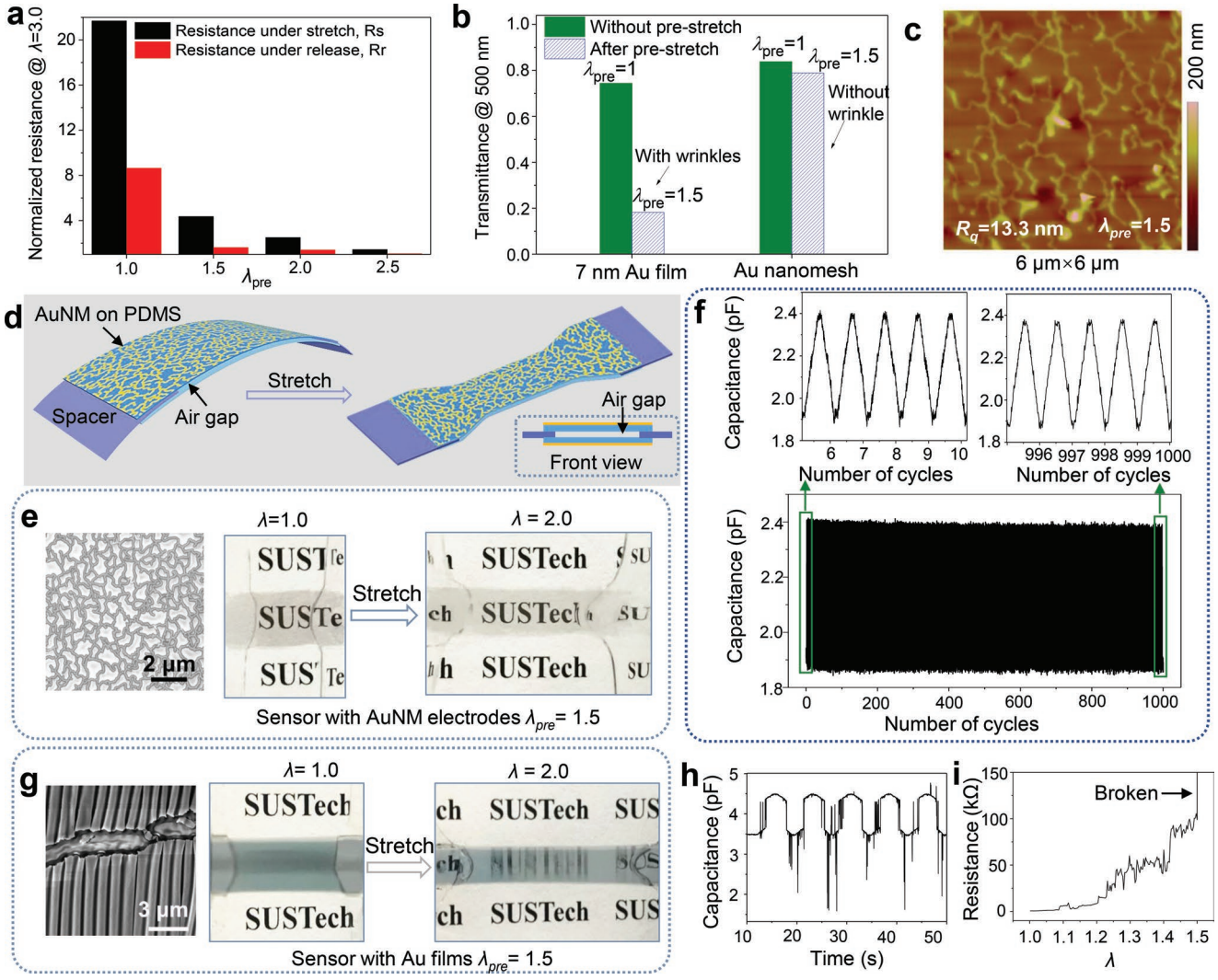

Figure 3. Performance of electrodes and stretchable strain sensors with a giant Poisson's effect. a) Change of resistance as a function of prestretch for the AuNM electrodes. b) Transmittance of the AuNM and a 7 nm thick Au film, both with and without prestrains. The prestrained AuNM shows little change in transmittance at $\lambda_{pre} = 1.5$, whereas the Au film has a significant change in transmittance at $\lambda_{pre} = 1.5$. c) AFM image of the AuNM at $\lambda_{pre} = 1.5$; no periodic wrinkles are seen. d) Schematic of a capacitive-type strain sensor using prestrained ($\lambda_{pre} = 1.5$) AuNM electrodes. e) Optical images of the sensor using prestrained ($\lambda_{pre} = 1.5$) AuNM electrodes at $\lambda = 1.0$ and 2.0, showing that the sensor always remains transparent during stretching. f) Optical images of a sensor applying Au nanofilms ($\lambda_{pre} = 1.5$) to replace the AuNMs. The sensor becomes opaque due to the formation of wrinkles as indicated in the SEM image on the left. g,h) Cyclic capacitive signals of the sensors with prestrained AuNMs (stretched to $\lambda = 2.0$) (g) and Au nanofilms (stretched to $\lambda = 1.2$) (h) as the electrodes, showing that the device with wrinkle-free AuNM electrodes is much more stable. i) Resistance of the Au nanofilm electrode ($\lambda_{pre} = 1.5$) as a function of stretch, indicating that the resistance changes significantly during stretching.

have a smaller increase in both stretched resistance (R_s) and released resistance (R_r). For example, at $\lambda = 3$, R_s increases by over 20 times for the sample without prestretch; while for the sample with $\lambda_{pre} = 2.5$, R_s increases by only 44%. The wrinkle-free and relatively smooth surfaces of the prestretched AuNM also lead to a much smaller scattering effect for visible light and the transmittance therefore changes little. Figure 3b shows that the AuNM loses only 3.7% (from 86.6% to 82.9% at 500 nm) of its transmittance in the case of $\lambda_{pre} = 1.5$. In comparison, the transmittance of a continuous 7 nm thick Au film on PDMS decreases from 65.8% to 26.3% at the same prestretch due to the scattering effect of periodic wrinkles or deep folds (Figure S6, Supporting Information). The low surface roughness of the prestrained AuNM is confirmed by AFM observations. For an AuNM with λ_{pre} of 1.5, the root-mean-square roughness (R_q) is only 13.3 nm (Figure 3c), which will not induce significant light scattering. Because the out-of-plane deformation only causes a local height change of the surface that is smaller than the feature size (or the width) of the Au nanowires,[30] the R_q is a far smaller value as compared with the wavelength of visible light, the roughness of wrinkled metal films (e.g., wrinkled graphene or wrinkled metal films), and the surface roughness of many other stretchable transparent electrodes, including Ag nanowire films and nanotrough networks (for which roughness values are typically larger than 100 nm).[31,32]

Stretchable and transparent electrodes free of surface instabilities can also significantly improve the performance of flexible electronic devices in several aspects. We show that a capacitive-type strain sensor that consists of two prestretched AuNM/PDMS electrodes ($\lambda_{pre} = 1.5$) and a thin air gap (the detailed device structure is shown in Figure 3d) can be stretched to large strains (up to 100%) while remaining highly transparent (Figure 3e). In contrast, a control sample that uses 7 nm thick Au films ($\lambda_{pre} = 1.5$) to replace the AuNMs exhibits high haze and poor direct transmittance due to the formation of surfaces wrinkles (Figure 3f) and, as a result, images behind the sensor cannot be identified. In addition, the device with prestrained AuNMs also presents advantages in sensing accuracy and durability: it exhibits a linear response to applied strain due to the incompressible nature of PDMS, and the signal remains stable after 1000 stretching/releasing cycles to 100% strain ($\lambda = 2$) (Figure 3g). On the other hand, the control sample with prestrained Au nanoscale films shows an unexpected signal waveform, as well as high noise with an amplitude comparable to the signal amplitude when stretched to a much smaller strain of 20% ($\lambda = 1.2$) (Figure 3h), which is due to unstable electrical conductance accompanied by the formation of cracks (Figure 3f,i).

The method of designing a stretchable network with a giant Poisson's effect to avoid surface instabilities is general and can be extended to other network geometries, as well as to applications other than electrodes and flexible electronics. We found that a variety of network geometries have effective Poisson's ratios larger than the critical value of $\frac{1-\lambda_{pre}^{-1}}{\sqrt{\lambda_{pre}}-1}$. Twelve kirigami patterns, including both regular and irregular mesh geometries (marked as P1–12 in **Figure 4**a) commonly used for electrodes, were laser-cut, and their effective Poisson's ratios were measured accordingly (Figure 4b). Figure 4b can be regarded as a phase diagram for which a wrinkling phase and a nonwrinkling phase are separated by the critical value of the Poisson's ratio. It can be seen that many structures, including the random network that mimics a silver nanowire network film (P11), fall well into the nonwrinkling regime, and thus, such sparse metal nanowire network electrodes do not wrinkle during deformation, as can be seen in the existing literature.[33,34] In addition, some geometries, e.g., the kirigami pattern mimicking our AuNM (P12), exhibit both a large Poisson's effect over a wide strain range and a large stretchability, and such geometries are ideal for wrinkle-free stretchable transparent electrodes.

It is interesting to note that some highly stretchable geometries (e.g., from P1 to P4) are within the wrinkling regime at small prestrains, but they move into the nonwrinkling regime as the prestrain increases. This indicates that wrinkles appear in such networks when the compressive strain or prestrain is small but will disappear when the prestrain increases beyond a critical value. This result seems to defy the common assumption that a larger prestrain or a larger compressive strain will more easily cause bilayer wrinkling, but it is valid for structures with a large Poisson's effect, which has not been discussed previously. We have experimentally confirmed this result: a Au nanonetwork with a geometry of P2 at a thickness of 40 nm (Figure 4c) released from a small prestretch of 1.1 exhibits surface wrinkles with a wavelength ≈1.3 μm (which agrees well with calculation),[35,36] as shown in Figure 4d and Figure S7 (Supporting Information). When λ_{pre} increases to 2.7, however, the wrinkles disappear and the network transforms to the nonwrinkling phase, for which an out-of-plane deformation of the ligaments that is significantly different from the surface wrinkles is observed (Figure 4e). Both the wrinkling and nonwrinkling phases result from the combined effect of nanokirigami and the mismatch of Poisson's ratios between the network and the substrate (Figure S8, Supporting Information). Here, paper kirigami mimicking the nanonetwork is used to understand the two phases. In the wrinkling regime ($\lambda_{pre} = 1.1$ or $\lambda = 1.05$ for the corresponding paper kirigami), the substrate squeezes the nanokirigami, forming surface wrinkles, and thus the nanonetwork has a morphology different from the corresponding paper kirigami. On the other hand, the nanokirigami is biaxially stretched by the substrate in the nonwrinkling regime ($\lambda_{pre} = 2.7$ or $\lambda = 1.65$ for the paper kirigami) and maintains the same geometry, similar to the corresponding paper kirigami. It should be noted that the out-of-plane deformation of the ligaments will also cause increased surface roughness. However, the height of the relief will not be larger than the width of the ligaments, and thus the surface roughness of the nanoscale network is limited. The results indicate that nanokirigami can be formed not only for freestanding structures,[20] but also for structures with an elastic substrate. The substrate will, in turn, regulate the kirigami structure depending on the effective Poisson's ratio.

We predict that the effect of the giant Poisson's ratio in preventing surface wrinkles is not only valid for flexible transparent electrodes and stretchable electronics, but may also be useful for other applications such as acoustics, advanced sensing, biomedical engineering, aerospace, and photonic crystals.[37–40] It should be noted that the stiff layer is not limited to 2D networks, but can be extended to 3D functional metastructures

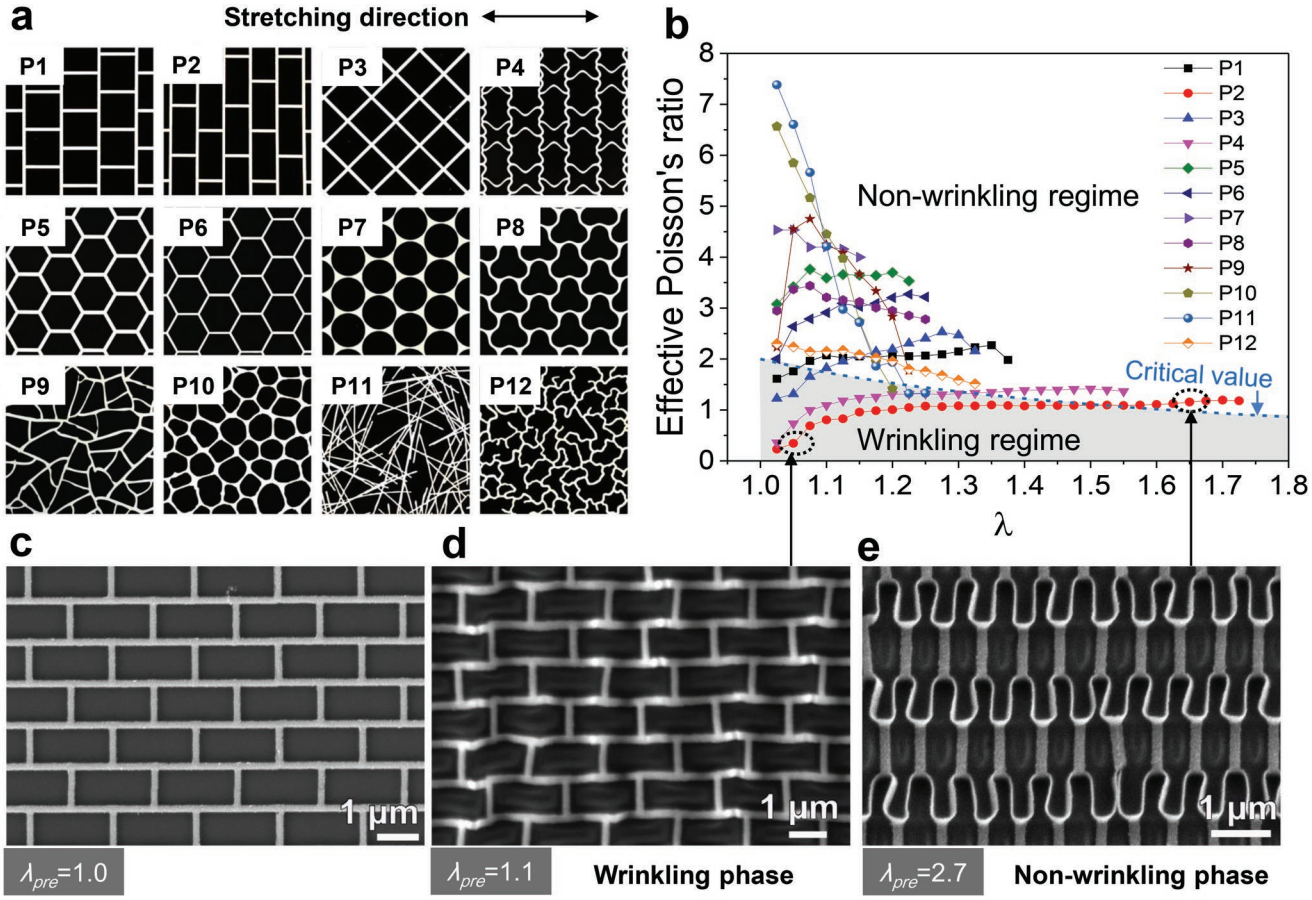

Figure 4. Large Poisson's effect in a variety of mesh structures. a) Paper kirigami structures with different geometries marked as P1–12. b) Effective Poisson's ratios of the meshes as a function of strain. Results are measured in the case of stretching the kirigami patterns along the horizontal direction. The critical Poisson's ratio is plotted as a reference. c–e) SEM images of an Au network with the geometry of P2 released with λ_{pre} = 1.0, 1.1, and 2.7, respectively. The substrate is PDMS. The Au network with λ_{pre} = 1.1 shows dense surface wrinkles, whereas the network with λ_{pre} = 2.7 exhibits out-of-plane deformation of the ligaments instead of surface wrinkles.

that exhibit large Poisson's ratios. Because Poisson's ratio is independent on the scale, the effect to prevent instabilities will be valid in not only nanoscale but also macroscale materials and structures, and thus this principle can find much broader applications.

We found that a metal/elastomer bilayer, upon compression (or releasing from prestretching), stretching, or bending, is free of surface instabilities when the metal layer has a large elastic limit (or is highly stretchable) and exhibits an effective Poisson's ratio larger than the critical condition of $\frac{1-\lambda_{pre}^{-1}}{\sqrt{\lambda_{pre}}-1}$. The principle has been verified in a AuNM that exhibits large stretchability as well as a giant Poisson's effect, and that shows no wrinkles on a prestretched substrate. The principle is believed to be general and can be applied to a variety of network electrodes and electronic devices, and it is of great significance for stretchable transparent electrodes and photoelectronic devices because it allows prestraining to significantly improve the stretchability of such nanoscale electrodes and devices while having little impact on their transparency and surface roughness. This work also shows that nanoscale kirigami can be formed and will be regulated by an elastic substrate, depending on the mismatch of effective Poisson's ratios between the network and the substrate. We also provide a new perspective to design materials and structures that demand instability-free surfaces, which are not limited only to flexible electronics, but also include mechanical structures, optical materials, biomedical materials, and others.

Experimental Section

Materials and Characterization: The AuNM was fabricated by using a method that we call grain boundary lithography.[30] The AuNM consists of serpentine ligaments, which form random holes with an average mesh size (M) close to 1 μm. The AuNM is ≈40 nm thick, with an area fraction of Au ≈0.2, and was deposited by e-beam evaporation. The Au nanonetwork shown in Figure 4 was fabricated by electron beam lithography. The PDMS substrate, which was made with a curing agent to base volumetric ratio of 1:10, has a Young's modulus of ≈1 MPa and a Poisson's ratio of 0.5. The transmittance of the samples was recorded with an Agilent Cary 5000 spectrometer. The scanning electron microscopy images were taken using an LOE 1525 scanning electron microscope and a TESCAN microscope. The atomic force microscopy images were taken using a Veeco D3100 machine. The optical images were taken using an Olympus Lext 4000 confocal microscope.

Laser Cutting of Kirigami Patterns and the Measurement of Poisson's Effect: Vector files (in dwg format) with designed patterns mimicking SEM images of transparent AuNMs and other networks were generated using DraftSight software. The corresponding kirigami patterns were made by laser cutting (Universal Laser Systems X-660) of thin sheets of printing paper. The kirigami patterns were then stretched, and the lengths as well as the lateral contractions were recorded during stretching to determine the effective Poisson's ratio based on Equation (2).

Fabrication and Measurement of Stretchable and Transparent Capacitive-Type Tactile Sensors: The device consists of two prestretched AuNM/PDMS bilayers (6 mm × 10 mm) sandwiching a thin air gap. The thickness of the PDMS substrate is ≈ 100 µm. The thickness of the air dielectric layer was determined by two PDMS spacers with a thickness of ≈ 500 µm placed at both sides of the sensor. The capacitance of the sensor was tested using an LCR meter (Keysight E4980AL) operated at 1 MHz.

Supporting Information

Supporting Information is available from the Wiley Online Library or from the author.

Acknowledgements

The work conducted at SUSTech was funded by the National Natural Science Foundation of China (No. 51771089), the "Science Technology and Innovation Committee of Shenzhen Municipality" (Grant Nos. JCYJ20170817111714314 and JCYJ20160613160524999), and the "Guangdong Innovative and Entrepreneurial Research Team Program" under Contract No. 2016ZT06G587. The authors thank the Materials Characterization and Preparation Center of SUSTech for preparing the samples.

Conflict of Interest

The authors declare no conflict of interest.

Keywords

flexible electrodes, kirigami, Poisson's effect, stretchability, transparency, wrinkles

Received: May 8, 2019
Revised: June 10, 2019
Published online: July 3, 2019

[1] S. Bae, H. Kim, Y. Lee, X. Xu, J.-S. Park, Y. Zheng, J. Balakrishnan, T. Lei, H. R. Kim, Y. I. Song, Y.-J. Kim, K. S. Kim, B. Özyilmaz, J.-H. Ahn, B. H. Hong, S. Iijima, *Nat. Nanotechnol.* **2010**, *5*, 574.
[2] D. H. Kim, N. Lu, R. Ma, Y. S. Kim, R. H. Kim, S. Wang, J. Wu, S. M. Won, H. Tao, A. Islam, K. J. Yu, T. Kim, R. Chowdhury, M. Ying, L. Xu, M. Li, H.-J. Chung, H. Keum, M. McCormick, P. Liu, Y.-W. Zhang, F. G. Omenetto, Y. Huang, T. Coleman, J. A. Rogers, *Science* **2011**, *333*, 838.
[3] D. J. Lipomi, M. Vosgueritchian, B. C. Tee, S. L. Hellstrom, J. A. Lee, C. H. Fox, Z. Bao, *Nat. Nanotechnol.* **2011**, *6*, 788.
[4] B. W. An, S. Heo, S. Ji, F. Bien, J.-U. Park, *Nat. Commun.* **2018**, *9*, 2458.
[5] J. Liu, T.-M. Fu, Z. Cheng, G. Hong, T. Zhou, L. Jin, M. Duvvuri, Z. Jiang, P. Kruskal, C. Xie, Z. Suo, Y. Fang, C. M. Lieber, *Nat. Nanotechnol.* **2015**, *10*, 629.
[6] G. Chen, N. Matsuhisa, Z. Liu, D. Qi, P. Cai, Y. Jiang, C. Wan, Y. Cui, W. R. Leow, Z. Liu, S. Gong, K.-Q. Zhang, Y. Cheng, X. Chen, *Adv. Mater.* **2018**, *30*, 1800129.
[7] Y.-Y. Chen, Y. Sun, Q.-B. Zhu, B.-W. Wang, X. Yan, S. Qiu, Q.-W. Li, P.-X. Hou, C. Liu, D.-M. Sun, H.-M. Cheng, *Adv. Sci.* **2018**, *5*, 1700965.
[8] J. Y. Chung, A. J. Nolte, C. M. Stafford, *Adv. Mater.* **2011**, *23*, 349.
[9] Y. Cao, J. W. Hutchinson, *J. Appl. Mech.* **2012**, *79*, 031019.
[10] J. Zang, S. Ryu, N. Pugno, Q. Wang, Q. Tu, M. J. Buehler, X. Zhao, *Nat. Mater.* **2013**, *12*, 321.
[11] M. Drack, I. Graz, T. Sekitani, T. Someya, M. Kaltenbrunner, S. Bauer, *Adv. Mater.* **2015**, *27*, 34.
[12] Y. Fang, Z. Wu, J. Li, F. Jiang, K. Zhang, Y. Zhang, Y. Zhou, J. Zhou, B. Hu, *Adv. Funct. Mater.* **2018**, *28*, 1705409.
[13] S. R. Dupont, M. Oliver, F. C. Krebs, R. H. Dauskardt, *Sol. Energy Mater. Sol. Cells* **2012**, *97*, 171.
[14] E. P. Chan, E. J. Smith, R. C. Hayward, A. J. Crosby, *Adv. Mater.* **2008**, *20*, 711.
[15] M. Yunusa, G. J. Amador, D.-M. Drotlef, M. Sitti, *Nano Lett.* **2018**, *18*, 2498.
[16] K. Ellmer, *Nat. Photonics* **2012**, *6*, 809.
[17] X. Wang, L. Zhi, K. Müllen, *Nano Lett.* **2008**, *8*, 323.
[18] M. G. P. Carbone, A. C. Manikas, I. Souli, C. Pavlou, C. Galiotis, *Nat. Commun.* **2019**, *10*, 1572.
[19] D. P. Dubal, N. R. Chodankar, D.-H. Kimc, P. Gomez-Romero, *Chem. Soc. Rev.* **2018**, *47*, 2065.
[20] S. Stauss, I. Honma, *Bull. Chem. Soc. Jpn.* **2018**, *91*, 492.
[21] K. Ariga, S. Watanabe, T. Mori, J. Takeya, *NPG Asia Mater.* **2018**, *10*, 90.
[22] C. F. Guo, Q. Liu, G. Wang, Y. Wang, Z. Shi, Z. Suo, C. W. Chu, Z. Ren, *Proc. Natl. Acad. Sci. USA* **2015**, *112*, 12332.
[23] M. K. Blees, A. W. Barnard, P. A. Rose, S. P. Roberts, K. L. McGill, P. Y. Huang, A. R. Ruyack, J. W. Kevek, B. Kobrin, D. A. Muller, P. L. McEuen, *Nature* **2015**, *524*, 204.
[24] D. Prall, R. S. Lakes, *Intl. J. Mech. Sci.* **1997**, *39*, 305.
[25] C. R. Weinberger, W. Cai, *J. Mater. Chem.* **2012**, *22*, 3277.
[26] P. Lee, P. Lee, J. Lee, H. Lee, J. Yeo, S. Hong, K. H. Nam, D. Lee, S. S. Lee, S. H. Ko, *Adv. Mater.* **2012**, *24*, 3326.
[27] Z. Niu, H. Dong, B. Zhu, J. Li, H. H. Hng, W. Zhou, X. Chen, S. Xie, *Adv. Mater.* **2013**, *25*, 1058.
[28] H. Li, T. Lv, H. Sun, G. Qian, N. Li, Y. Yao, T. Chen, *Nat. Commun.* **2019**, *10*, 536.
[29] R. Nur, N. Matsuhisa, Z. Jiang, M. O. G. Nayeem, T. Yokota, T. Someya, *Nano Lett.* **2018**, *18*, 5610.
[30] C. F. Guo, T. Sun, Q. Liu, Z. Suo, Z. Ren, *Nat. Commun.* **2014**, *5*, 3121.
[31] H. Wu, D. Kong, Z. Ruan, P.-C. Hsu, S. Wang, Z. Yu, T. J. Carney, L. Hu, S. Fan, Y. Cui, *Nat. Nanotechnol.* **2013**, *8*, 421.
[32] L. Hu, H. S. Kim, J. Y. Lee, P. Peumans, Y. Cui, *ACS Nano* **2010**, *4*, 2955.
[33] X. Ho, J. N. Tey, W. Liu, C. K. Cheng, J. Wei, *J. Appl. Phys.* **2013**, *113*, 044311.
[34] C. F. Guo, Y. Lan, T. Sun, Z. Ren, *Nano Energy* **2014**, *8*, 110.
[35] C. M. Stafford, C. Harrison, K. Beers, A. Karim, E. J. Amis, M. R. Vanlandingham, H.-C. Kim, Willivolksen, R. D. Miller, E. Simonyi, *Nat. Mater.* **2004**, *3*, 545.
[36] W. T. S. Huck, N. Bowden, P. Onck, T. Pardoen, J. W. Hutchinson, G. M. Whitesides, *Langmuir* **2000**, *16*, 3497.
[37] Y. Wan, Y. Wang, C. F. Guo, *Mater. Today Phys.* **2017**, *1*, 61.
[38] A. Clausen, F. Wang, J. S. Jensen, O. Sigmund, J. A. Lewis, *Adv. Mater.* **2015**, *27*, 5523.
[39] R. H. Baughman, S. O. Dantas, S. Stafström, A. A. Zakhidov, T. B. Mitchell, D. H. Dubin, *Science* **2000**, *288*, 2018.
[40] M. Farsari, B. N. Chichkov, *Nat. Photonics* **2009**, *3*, 450.